Development of spin-coated Si/TiOx/Pt/TiOx electrodes for the electrochemical ozone production

Ahmad M. Mohammad [a,b], Kenta Kitsuka [a,c], Aboubakr M. Abdullah [a,b], Mohamed I. Awad [a,b], Takeyoshi Okajima [a], Kazuhiro Kaneda [c], Mineo Ikematsu [c], Takeo Ohsaka [a,*]

[a] *Department of Electronic Chemistry, Interdisciplinary Graduate School of Science and Engineering, Tokyo Institute of Technology, 4259 Nagatsuta, Midori-ku, Yokohama 226-8502, Japan*
[b] *Chemistry Department, Faculty of Science, Cairo University, P.O. 12613 – Giza, Egypt*
[c] *Human Ecology Research Center, Sanyo Electric Co., Ltd., 1-1-1 Sakata, Oizumi, Ora, Gunma 370-0596, Japan*

ARTICLE INFO

ABSTRACT

A novel electrode having the compositional sequence Si/TiOx/Pt/TiOx was developed for ozone electrogeneration. The spin-coating method, the sputtering deposition technique, and a post-annealing procedure were all combined to assemble the electrode composition. A two-compartment electrolytic cell separated by a Nafion membrane was used to generate ozone galvanostatically. The X-ray photon electron spectroscopy (XPS) and atomic force microscopy (AFM) were used to reveal the electrode composition and morphology. The influence of several factors including the electrode's annealing temperature, the electrolyte composition, and the electrolysis' current density on the efficiency of ozone production was investigated. A maximum ozone generation efficiency of 2.5% was obtained at 74 mA cm^{-2} at room temperature. Interestingly, the electrode preserved (ca. 80%) of its original activity to produce ozone after 50 h of continues electrolysis at 74 mA cm^{-2} at room temperature.
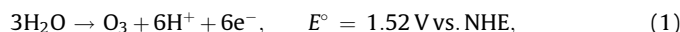
1. Introduction

Ozone is currently attracting a considerable interest due to its wide applications in chemical, environmental, pulp, food, and recently in medical industries [1–3]. Unlike chlorine, ozone does not generate harmful residues and is about six times as strong as chlorine in terms of oxidizing power. In water treatment, ozone is more interesting due to its relatively short half-life even at normal temperatures. Combinations of ozone and hydrogen peroxide or ultraviolet radiation in water can generate powerful oxidants useful in advanced oxidation processes, AOP [4]. Hence, the ozone production has recently glittered as an attractive prospect [5].

Practically, two approaches have long been used to generate ozone; the UV-light and corona-discharge [6]. The UV-light approach can only be used when small amounts of ozone are desired. Although more complicated and expensive, the corona-discharge approach is able to produce much higher amounts of ozone. Recently, the electrochemical ozone production, EOP, from water electrolysis, attracted a deal of attention due to its low cost and simplicity [7–10]. In this process, ozone is produced at the anode and hydrogen gas is produced at the cathode of an electrolytic cell according to the following equations:

$$3H_2O \rightarrow O_3 + 6H^+ + 6e^-, \qquad E^\circ = 1.52\ V\ vs.\ NHE, \qquad (1)$$

$$2H^+ + 2e^- \rightarrow H_2, \qquad E^\circ = 0.0\ V. \qquad (2)$$

However, the anodic reaction is always competed by the oxygen evolution reaction (OER);

$$2H_2O \rightarrow O_2 + 4H^+ + 4e^-, \qquad E^\circ = 1.23\ V\ vs.\ NHE. \qquad (1a)$$
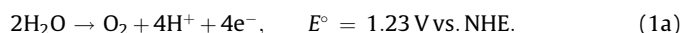
Hence, to generate ozone, an optimization is required to slow down the oxygen evolution reaction and achieve the highest ozone yield and efficiency. Basically, several factors are able to influence the EOP such as the anode materials (high oxygen overpotential anodes are favorable to minimize the oxygen evolution), the electrolyte type, concentration, and acidity (the adsorption mechanism may change by adding anions of a high adsorption tendency), and the electrolysis parameters and temperature

(lowering the temperature at the anode/electrolyte interface will likely decrease the thermal dissociation of ozone) [11–14].

Lead dioxide, for long time, was the best candidate for EOP, and a current efficiency of more than 7% was reported at a current density of 600 mA/cm^2 in 5 M H$_2$SO$_4$ [11]. The size and morphology of lead dioxide particles could also greatly influence the electrode performance [15,16]. However, the use of lead-containing materials is unsafe and currently prohibited. Platinum, on the other hand, is much less efficient than lead dioxide to produce ozone (less than 2% at a current density of 400 mA/cm^2) [11]. This efficiency was improved to 8.5% by lowering the temperature to −67 °C in 5 M eutectic H$_2$SO$_4$ [11].

Recently, tantalum–platinum composites have appeared promising for EOP; a current efficiency of up to 6% at 20 mA cm^{-2} was reported at RT [10,13,17–19]. Nevertheless, the electrode material is highly expensive and the preparation procedures are complicated and lengthy. Titanium-based composites have next been proposed as cheap materials for EOP [20]. Titanium oxides participate in a broad range of industrial applications [21–23], and recently exhibited a reasonable catalysis towards oxygen reduction [24,25], and water splitting [26].

Herein, we report on the electrocatalytic activity of a titanium oxide–platinum composite electrode prepared by the spin-coating and sputtering methods towards EOP in perchloric acid. The electrode's performance is correlated to the electrode's composition and the parameters of electrolysis.

2. Experimental

2.1. Electrode preparation

A spin-coating method (Kyowariken, K-359 S-1, Japan) was used to deposit the titanium precursors on the Si/TiOx/Pt substrates. Ti (3%) metallic precursors were purchased from Koujundo Kagaku. Co. Ltd., Japan. The following procedure was applied to prepare the Si/TiOx/Pt substrate. An RF sputtering machine (ULVAC, Inc.) was used to deposit a titanium oxide (TiOx) film on a Si substrate for 10 min at room temperature (RT) under a total gas pressure of 0.6 Pa (Ar/O$_2$ ratio = 0.48/0.52) and an RF power density of 6.4 W/cm^2. This was done to strengthen the adhesion of the Si substrate and the Pt film, and to suppress the mutual diffusion of Si and Pt. Next, the Pt film was deposited on the TiOx layer, hitherto deposited on the Si substrate, for 1 min at RT under an Ar gas pressure of 0.7 Pa and RF power density of 4.8 W/cm^2. The substrate was then subjected to spin-coating with titanium precursors. Two-step spinning at 1000 rpm for 10 s followed by another one at 3000 rpm for 30 s was done to coat the Si/TiOx/Pt substrate with titanium precursors. After that, the electrode was left to dry in air at RT for 10 min and next at 200 °C for another 10 min. The average thickness of the Ti layer was ∼60 nm. Finally, the electrodes were annealed at different temperatures (550, 600, and 650 °C) for 10 min in air.

2.2. Electrochemical measurements

The cyclic voltammograms (CVs), measured at 0.1 V/s in 10 mM HClO$_4$, and the linear sweep voltammograms (LSVs), measured at 5 mV/s in 10 mM HClO$_4$, were all done in N$_2$ atmosphere using a BAS 100 B/W electrochemical analyzer. The working electrode and the counter electrode (a platinum spiral wire) were separated by porous glass. A Ag/AgCl (KCl sat.) electrode was used as the reference electrode.

Electrogeneration of O$_3$ was performed galvanostatically at RT in HClO$_4$ acid in a Nafion membrane cell. The cell was of two compartments separated by a Nafion membrane. Ag/AgCl (KCl sat.) was used as a reference electrode. Ohmic drop was minimized

using a Luggin capillary approaching the working electrode. The counter electrode was Pt electrode of a large surface area. Electrode area was determined before electrolysis based on the charge associated with the hydrogen underpotential deposition peaks (220 μC/cm^2) [27].

A simple and rapid potentiometric method with a high sensitivity and selectivity was used in this study to measure the concentration of gaseous and soluble ozone [28,29]. In this method, a Pt electrode was used as an indicator electrode and the I$_3^-$/I$^-$ redox couple was used as a probing potential buffer. The analysis is based on measuring the change of the open circuit potential of the indicator electrode that results when the oxidant reacts with I$^-$. The following Nernstian equation was developed to estimate the change in potential, ΔE, when an oxidant, Ox, gains two electrons in the oxidation reaction of I$^-$ at 25 °C under the condition of being the initial concentration of iodide, [I$^-$]$_o$, much greater than that of the oxidant, [Ox].

$$\Delta E, \text{mV} = 29.6 \log\{(1 + ([Ox]/[I_3^-]_o)\}, \tag{3}$$

where [I$_3^-$]$_o$ is the initial concentration of I$_3^-$. The O$_3$ gas escaped from the cell during electrolysis was in-situ analyzed by passing into an I$_3^-$/I$^-$ potential buffer solution. The electrolytic cell is well designed to ensure a complete trapping of O$_3$ gas into the potential buffer solution. The current efficiency was determined according to Faraday's law based on Eq. (1) using the total concentration of O$_3$ both dissolved in the electrolyte solution and in the gas phase.

2.3. Electrode characterization

The X-ray photon electron spectroscopic (XPS) analysis was performed using an ESCA-3400 electron spectrometer (SHIMADZU) having a non-monochromatic Mg Kα ($h\nu$ = 1253.6 eV) X-ray source, with power given by the emission of 20 mA at a voltage of 10 kV. The atomic force microscopic (AFM) images were pictured ex-situ in the direct contact mode using the AFM (Nanoscale Hybrid Microscope VN–8000—KEYENCE) microscope.

3. Results and discussion

3.1. Effect of annealing temperature

Titanium oxide electrodes are usually prepared either by dry methods such as sputtering [30] and chemical vapor deposition methods [31] or by wet processes such as dip coating [32] sol–gel [33,34] spray coating [35] and spin-coating methods [36]. Wet-processing operations are, indeed, easier and require no particular equipment. However, the produced oxide is usually amorphous, and thermal treatments are required to obtain a uniform oxide film with a desired structural and electrocatalytic characteristics [37]. Figs. 1 and 2 show the CVs and LSVs in 10 mM HClO$_4$ acid solution at three different spin-coated Si/TiOx/Pt/TiOx electrodes after annealing at 550 (a), 600 (b) and 650 °C (c). The characteristic behavior of a polycrystalline Pt electrode is clearly shown in the CVs of the three electrodes; Pt oxidation, which extends over a wide range of potential, is coupled with the reduction peak at ca. 0.30–0.35 V (vs. Ag/AgCl). This couple corresponds to the solid-state surface redox transition (SSSRT) involving Pt/PtO. In addition, ill-defined peaks for the hydrogen adsorption/desorption are shown in the potential range from 0.0 to −0.2 V vs. Ag/AgCl. This behavior in Fig. 1 indicates that the platinum layer underneath the spin-coated titanium oxide layer is exposed to the electrolyte. In other words, the oxide film has some cracks. A similar porous structure has previously been observed for tantalum oxide films deposited on platinum using the sol–gel method [13]. This may explain the illness of the hydrogen adsorption/desorption peaks
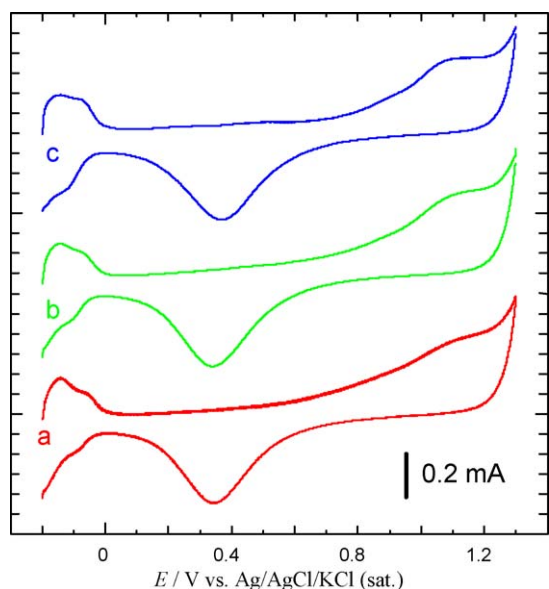
Fig. 1. The cyclic voltammograms in 10 mM HClO$_4$ solution under N$_2$ atmosphere at three Si/TiOx/Pt/TiOx electrodes annealed at (a) 550, (b) 600 and (c) 650 °C. Potential scan rate: 0.1 V/s.

Fig. 2. The linear sweep voltammograms in 10 mM HClO$_4$ solution under N$_2$ atmosphere at three Si/TiOx/Pt/TiOx electrodes annealed at (a) 550, (b) 600 and (c) 650 °C. Potential scan rate: 1 mV/s. The surface area is normalized based on the real surface area.
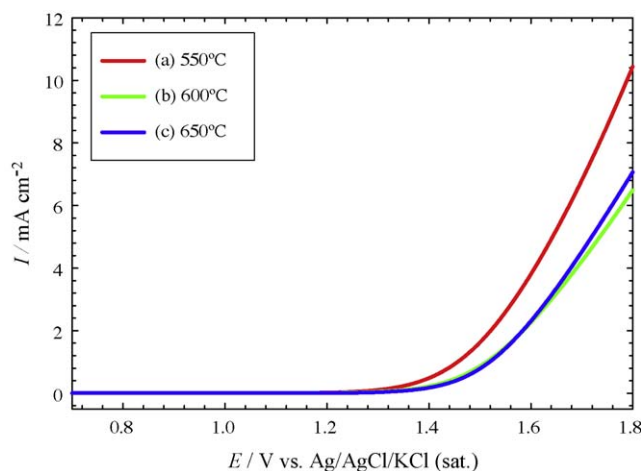
that probably resulted from accumulating gas bubbles in the pores of the TiOx film. In fact, TiOx/Pt electrodes have shown an enhancement for the hydrogen spillover as previously reported by Malevich et al. [38]. The LSVs curves in Fig. 2 indicate a difference in the onset potential of the oxygen evolution of the electrode annealed at 550 °C (~1.46 V vs. Ag/AgCl) and the other two electrodes (~1.52 V vs. Ag/AgCl). In other words, oxygen evolves early (~60 mV less) if the electrode is annealed at 550 °C. In turn, for the sake of minimizing the oxygen evolution, the use of 550 °C as an annealing temperature for this electrode in EOP is disfavored. The rate of oxygen evolution would also be considered when comparing the performance of a set of electrodes towards EOP. The lower rate of oxygen evolution is often favored in EOP technology. As shown in Fig. 2, the rate of oxygen evolution of the electrode annealed at 600 °C is lower than that of the other electrode annealed at 650 °C, particularly at high potentials that are typically used for EOP. Based on the above observations, one can predict that the electrode annealed at 600 °C will be the best among the three electrodes for EOP.

Table 1
Effect of annealing temperature on the ozone concentration and current efficiency. Electrolysis is done by applying 74 mA/cm^2 for 5 min in 10 mM HClO$_4$ acid. The surface area is normalized based on the real surface area.

$T_{annealing}$, °C	O$_3$ concentration, μM	O$_3$ current efficiency, %
550	7.5	1.2
600	15.3	2.5
650	9.8	1.6

In parallel, the EOP have been investigated using the same electrodes annealed at 550, 600, and 650 °C. Table 1 lists the concentrations and efficiencies of ozone generated galvanostatically at 74 mA/cm^2 for 5 min in 10 mM HClO$_4$ solution at RT. As expected above, the data in Table 1 shows that the electrode annealed at 600 °C is more efficient than the other two electrodes. The ozone yield and efficiency of this electrode were at least two times higher than those of the other two electrodes. We believe that the reason of favoring the annealing temperature of 600 °C might be understood within the framework of the O–Ti phase diagram. In order to understand this behavior, we have measured the XPS spectra for the three electrodes to reveal their surface composition.

Fig. 3 shows the Ti 2p XPS spectra of the Si/TiOx/Pt/TiOx electrodes annealed at temperatures 550 (a), 600 (b) and 650 °C (c). The data revealed the existence of several phases of titanium oxides in the three electrodes. The concentration of these phases depended on the annealing temperature. Titanium oxides can, indeed, exist in multiple phases and several phases can, moreover, coexist under certain conditions [39–41]. The annealing temperature and time are very critical in identifying the relative concentrations of these phases in the oxide. An XPS investigation by Boffa et al. [42] pointed out that annealing of titanium oxide films, grown by vapor phase deposition on platinum substrate, in oxygen atmosphere in the temperature range between 300 and 1000 °C for 5 min affects greatly the total (Ti^{4+} + Ti^{3+}) titanium and the relative Ti^{3+} contents. Our XPS data indicated that the Ti^{4+} (TiO$_2$) was the major component in all the electrodes whatever was the annealing temperature. The Ti doublet at 458.8 and 464 eV is assigned to 2p$_{3/2}$ and 2p$_{1/2}$, respectively [41,42]. Lower quantities of Ti^{3+} phase also existed as the peaks at 456 eV (2p$_{3/2}$) and 462 eV
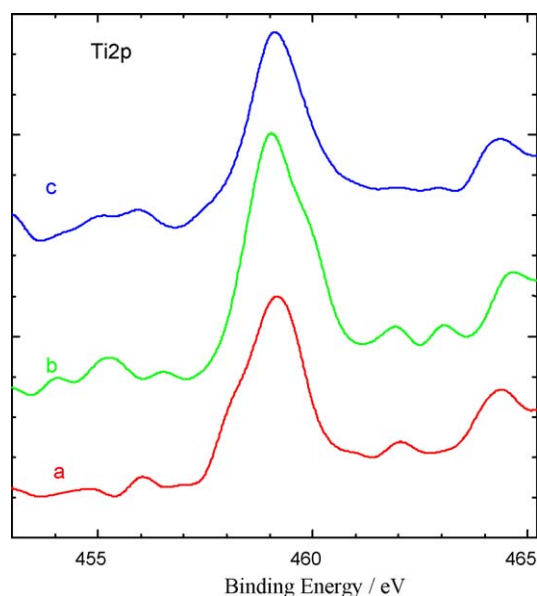

Fig. 3. The Ti 2p XPS spectra of the Si/TiOx/Pt/TiOx electrodes at different annealing temperatures (a) 550, (b) 600 and (c) 650 °C.

($2p_{1/2}$) indicate [41,42]. These peaks are shifted little to higher binding energies in case of the sample annealed at 600 °C (see curve (b)) to appear at 456.5 and 463.5 eV. A significant decrease in the Ti^{3+} content was observed with increasing the annealing temperature from 550 to 600 °C, in agreement with Boffa et al. [42] but very little amount of Ti^{3+} was detected when the sample was annealed at 650 °C. In addition, well-defined peaks at ~455.5 and 462 eV were only observed in the sample annealed at 600 °C, and are likely assigned to the TiO phase [41]. A similar but broader peak appeared with lower intensity for the sample annealed at 650 °C. The peak around 454 eV in curve b is assigned to metallic Ti [41]. From the XPS data analysis, it seems for us that the existence of small quantities of Ti^{2+} phase, in addition to Ti^{3+} and Ti^{4+} phases in the sample annealed at 600 °C is responsible for the enhancement of the electrocatalytic activity of this sample towards EOP. Hereafter, 600 °C will be selected as the optimum annealing treatment.

3.2. Effect of the electrolyte concentration

The effect of the electrolyte ($HClO_4$ acid) concentration on the ozone concentration and efficiency is further investigated for one of the electrodes annealed at 600 °C. Electrolysis was performed in 1, 10 and 100 mM $HClO_4$ acid solution at RT galvanostatically for 5 min at 74 mA cm^{-2}. By lowering the electrolyte concentration, we observed a significant increase in the overall cell potential but little increase in the potential was observed at the working electrode. The increase in the cell potential is likely due to the increase in the iR drop of the electrolyte. However, no significant change in the ozone concentration and efficiency was observed within this range of electrolyte concentrations (see Table 2).

3.3. AFM investigation

Viewing topography by itself is very informative in surface deformations in various materials. Surface roughness, in particular, is an important factor that influences the physicochemical properties of materials. Characterization of surface roughness involves two steps: instrumental measurement and quantification of the surface roughness. The latter includes two attributes: roughness heights and lateral dimensions. Fig. 4 represents high-resolution three-dimensional AFM (contact mode) images of one of the electrodes annealed at 600 °C before and after ozone generation at 74 mA cm^{-2} for 5 min in 10 mM $HClO_4$. The AFM pictures did not reveal a significant difference in the surface morphology of the electrodes before and after EOP. In addition, very close roughness factors were obtained for both measurements (about 0.06% increase in the surface roughness was observed after ozone generation). This indicates that ozone generation at 74 mA cm^{-2} does not damage the electrode and, therefore, it can further maintain reasonable electrocatalytic activity.

3.4. Effect of current density

We have further examined the effect of current density employed in EOP on the ozone concentrations and efficiencies. In Fig. 5, the
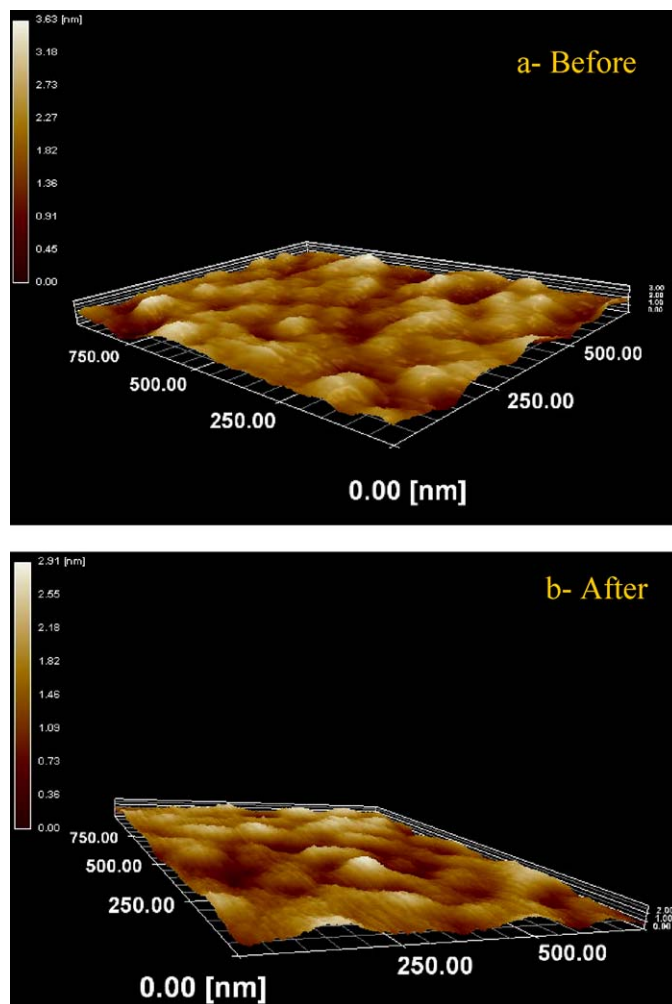

Fig. 4. Three-dimensional atomic force microscopy image (contact-mode) for one of the Si/TiOx/Pt/TiOx electrodes (a) before and (b) after electrolysis at 74 mA/cm^2 for 5 min in 10 mM $HClO_4$ acid.

concentration and efficiency of ozone generated in 10 mM $HClO_4$ at RT galvanostatically for 5 min are plotted as a function of the current density used in EOP. The amount of ozone increased in a semi-linear fashion with the current density. However, a maximum was
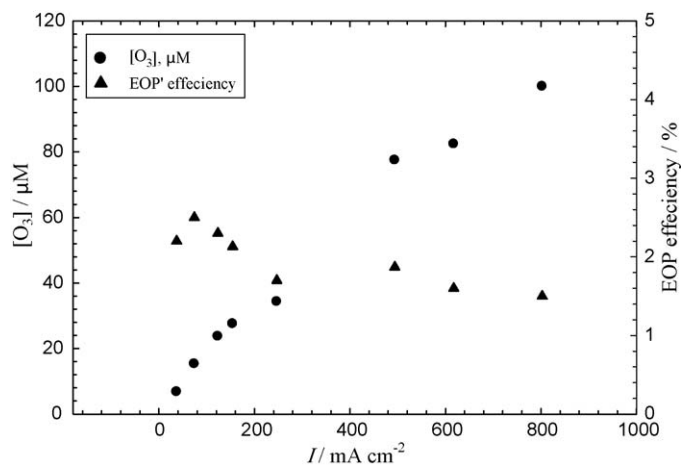
Table 2
Effect of electrolyte ($HClO_4$) concentration on the ozone concentration and current efficiency. Electrolysis is done by applying 74 mA/cm^2 for 5 min in different concentrations of $HClO_4$ acid. The surface area is normalized based on the real surface area.

[$HClO_4$], mM	O_3 concentration, μM	O_3 current efficiency, %
1.0	12.9	2.1
10.0	15.3	2.5
100.0	10.1	1.6

Fig. 5. Effect of current density on the EOP yield and current efficiency. Electrolysis was done by applying different current densities for 5 min in 10 mM $HClO_4$ acid at RT.
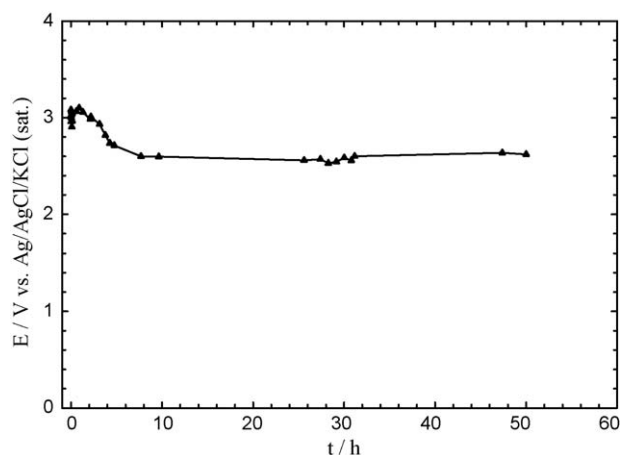
Fig. 6. Change in the potential of a Si/TiOx/Pt/TiOx electrode with electrolysis time. Electrolysis was done galvanostatically at 74 mA/cm^2 in 10 mM HClO$_4$ acid.

observed in the current efficiency at about 74 mA cm^{-2}. The decrease of efficiency with increasing the electrolysis current can be attributed to two reasons. The first is the increase in the local heating at the vicinity of the electrode with increasing the current. The increase in the current density was always accompanied by an increase in the cell voltage and the electrolyte temperature. In fact, the anode surface temperature rather than the bulk electrolyte temperature is critical in ozone synthesis. As the heating effect at the anode is roughly proportional to the square of current density, temperature discrepancies can become significant at higher current densities [11]. Increasing the local heating with the current density will definitely increase the rate of ozone decomposition, and therefore, the efficiency decreases. The second reason is perhaps the competition of other side reactions with EOP. By increasing the electrolysis current, the observed anodic potential increases and both the rates of OER and EOP are expected to increase. The electrode material and electrolyte are among the factors that determine the relative rates of both reactions. In fact, the electrolyte composition influences the EOP efficiency by changing the anion adsorption mechanism at the electrode surface, which further affects the activation energy and electrode kinetics of OER and EOP [14,43]. The influence of the anion adsorption becomes more pronounced at higher overpotentials, where a stronger interaction between the electrode surface and the anions takes place, thus leading to a considerable change in the apparent electronic transfer coefficient [14,43]. In the current investigation (utilizing TiOx electrodes and perchloric acid solution), we believe that high electrolysis currents increase the active sites for OER on the expense of EOP speeding up the OER and lowering the rate of EOP. Therefore the efficiency of EOP decreases with current in the high current region. Similarly, the ozone current efficiency decreased with the generation current density in sulfuric acid, phosphoric and fluoride containing solutions on lead dioxide electrodes [11]. Therefore, a maximum current efficiency (2.5%) was obtained at 74 mA cm^{-2} for the Si/TiOx/Pt/TiOx electrode in 10 mM HClO$_4$ at RT. This efficiency is almost comparable to that obtained previously on β-PbO$_2$ in 6 M HClO$_4$ solution (3.5% at 0 °C and 0.90 A cm^{-2}) [14].

3.5. Stability investigation

The stability of the electrode is an important criterion especially when it is used at a high anodic potential such as in O$_3$ generation. The stability of the electrode prepared at 600 °C was inferred by measuring the change in the electrode potential with time upon applying a constant current of 74 mA cm^{-2} (a current at which the highest efficiency was obtained) in 10 mM HClO$_4$ (see Fig. 6). The

potential decreased at the beginning and then remained fairly constant for about 50 h. We have examined the efficiency of EOP before and after this long electrolysis to evaluate the electrode stability. A little change in the EOP efficiency was observed after (efficiency ca. 2.0%) compared to the original efficiency before (efficiency ca. 2.5%) the long electrolysis experiment. This means that the electrode is maintaining about 80% of its original activity to produce ozone after 50 h continues electrolysis. The performance of the electrode may be improved if long but disconnected use of the electrode is desired. Understanding the details of the EOP mechanism is under investigation.

4. Conclusions

The spin-coating, and sputtering deposition techniques were combined to assemble a new electrode with the compositional sequence Si/TiOx/Pt/TiOx for ozone electrogeneration. Ozone was synthesized galvanostatically in a two-compartment electrolytic cell separated by a Nafion membrane. The effects of several factors including the electrode's annealing temperature, the electrolyte composition, and the electrolysis current density were investigated. A temperature of 600 °C, a concentration of 10 mM of HClO$_4$ solution and 74 mA cm^{-2} were found optimum for EOP in the current study. A maximum ozone generation efficiency of 2.5% at 74 mA cm^{-2} was obtained at RT. The electrode effectiveness towards EOP is decreased a little with continuous electrolysis for about 5 h and then remained almost constant for 50 h. Further work is necessary to achieve an understanding for the mechanism of ozone generation at this electrode.

References

[1] L. James, A.K. Puniya, V. Mishra, K. Singh, J. Sci. Ind. Res. 61 (2002) 504–509.
[2] M. Bortman, P. Brimblecombe, M.A. Cunningham, W.P. Cunningham, W. Freedman (Eds.), Environmental Encyclopedia, Gale, 2003.
[3] V. Bocci, N. Di Paolo, Ozone Sci. Eng. 26 (2004) 195–205.
[4] P. Tatapudi, J.M. Fenton, J. Electrochem. Soc. 141 (1994) 1174–1178.
[5] K. Arihara, C. Terashima, A. Fujishima, J. Electrochem. Soc. 154 (2007) 71–75.
[6] J. Chen, J.H. Davidson, Plasma Chem. Plasma Process. 23 (2003) 501–518.
[7] L.M. Da Silva, L.A. De Faria, J.F.C. Boodts, Pure Appl. Chem. 73 (2001) 1871–1884.
[8] L.M. Da Silva, M.H.P. Santana, J.F.C. Boodts, Quim. Nova 26 (2003) 880–888.
[9] L.M. Da Silva, L.A. De Faria, J.F.C. Boodts, Electrochim. Acta 48 (2003) 699–709.
[10] K. Kaneda, M. Ikematsu, K. Kitsuka, M. Iseki, H. Matsuura, T. Higuchi, T. Hattori, T. Tsukamoto, M. Yasuda, Jpn. J. Appl. Phys. Part 1 45 (2006) 6417–6419.
[11] P.C. Foller, C.W. Tobias, J. Electrochem. Soc. 129 (1982) 506–515.
[12] P.C. Foller, M.L. Goodwin, Ozone Sci. Eng. 6 (1984) 29–36.
[13] M.I. Awad, S. Sata, K. Kaneda, M. Ikematsu, T. Okajima, T. Ohsaka, Electrochem. Commun. 8 (2006) 1263–1269.
[14] D.V. Franco, L.M. Da Silva, W.F. Jardima, J.F.C. Boodts, J. Braz. Chem. Soc. 17 (2006) 746–757.
[15] J. Wang, X. Jing, Electrochemistry (Japan) 74 (2006) 539–543.
[16] J. Wang, X. Li, L. Guo, X. Luo, Appl. Surf. Sci. 254 (2008) 6666–6670.
[17] K. Kaneda, M. Ikematsu, M. Iseki, D. Takaoka, T. Higuchi, T. Hattori, T. Tsukamoto, M. Yasuda, Chem. Lett. 34 (2005) 1320–1321.
[18] K. Kaneda, M. Ikematsu, Y. Koizumi, H. Minoshima, T. Rakuma, D. Takaoka, M. Yasuda, Electrochem. Solid-State Lett. 8 (2005).
[19] K. Kaneda, M. Ikematsu, M. Iseki, D. Takaoka, T. Higuchi, T. Hattori, T. Tsukamoto, M. Yasuda, Jpn. J. Appl. Phys. Part 1 45 (2006) 5154–5162.
[20] A.M. Mohammad, K. Kitsuka, K. Kaneda, M.I. Awad, A.M. Abdullah, M. Ikematsu, T. Ohsaka, Chem. Lett. 36 (2007) 1046–1047.
[21] Y.-Q. Li, S.-Y. Fu, G. Yang, M. Li, J. Non-Cryst. Solids 352 (2006) 3339–3342.
[22] K.-S. Lee, I.-S. Park, Scripta Mater. 48 (2003) 659–663.
[23] L.L. Amy, G. Lu, T. John, Chem. Rev. 95 (1995) 725–758.
[24] J.-H. Kim, A. Ishihara, S. Mitsushima, N. Kamiya, K.-I. Ota, Electrochim. Acta 52 (2007) 2492–2497.
[25] S.V. Mentus, Electrochim. Acta 50 (2004) 27–32.
[26] W. Nam, G.Y. Han, J. Chem. Eng. Jpn. 40 (2007) 266–269.
[27] S.V. Mentus, Electrochim. Acta 50 (2005) 3609–3615.
[28] M.I. Awad, T. Oritani, T. Ohsaka, Anal. Chem. 75 (2003) 2688–2693.

[29] M.I. Awad, T. Ohsaka, Electrochem. Commun. 6 (2004) 1135–1140.
[30] K. Takagi, T. Makimoto, H. Hiraiwa, T. Negishi, J. Vac. Sci. Technol. A 19 (2001) 2931–2935.
[31] G.A. Battiston, R. Gerbasi, M. Porchia, A. Marigo, Thin Solid Films 239 (1994) 186–191.
[32] T. Yoko, A. Yuasa, K. Kamiya, S. Sakka, J. Electrochem. Soc. 138 (1991) 2279–2285.
[33] A. Tsuzuki, H. Murakami, K. Kani, S. Kawakami, Y. Torii, J. Mater. Sci. Lett. 9 (1990) 624–626.
[34] U. Selvaraj, A.V. Prasadarao, S. Komarneni, R. Roy, J. Am. Ceram. Soc. 75 (1992) 1167–1170.
[35] R. Wang, K. Hashimoto, A. Fujishima, M. Chikuni, E. Kojima, A. Kitamura, M. Shimohigoshi, T. Watanabe, Adv. Mater. 10 (1998) 135–138.
[36] M. Anast, A. Jamting, J.M. Bell, B. Ben-Nissan, Thin Solid Films 253 (1994) 303–307.

[37] H. Koyama, M. Fujimoto, T. Ohno, H. Suzuki, J. Tanaka, J. Am. Ceram. Soc. 89 (2006) 3536–3540.
[38] D.V. Malevich, V.B. Drozdovich, I.M. Zharskii, Stud. Surf. Sci. Catal. 112 (1997) 359–366.
[39] J. Pouilleau, D. Devilliers, F. Garrido, S. Durand-Vidal, E. Mahe, Mater. Sci. Eng.: B 47 (1997) 235–243.
[40] T. Godfroid, R. Gouttebaron, J.P. Dauchot, P. Leclere, R. Lazzaroni, M. Hecq, Thin Solid Films 437 (2003) 57–62.
[41] C.E.B. Marino, P.A.P. Nascente, S.R. Biaggio, R.C. Rocha-Filho, N. Bocchi, Thin Solid Films 468 (2004) 109–112.
[42] A.B. Boffa, H.C. Galloway, P.W. Jacobs, J.J. Benitez, J.D. Batteas, M. Salmeron, A.T. Bell, G.A. Somorjai, Surf. Sci. 326 (1995) 80–92.
[43] L.M. Da Silva, D.V. Franco, L.A. De Faria, J.F.C. Boodts, Electrochim. Acta 49 (2004) 3977–3988.